Geophysical Research Letters

RESEARCH LETTER
10.1029/2019GL083095

The Effect of QBO Phase on the Atmospheric Response to Projected Arctic Sea Ice Loss in Early Winter

Zachary Labe[1], **Yannick Peings**[1], **and Gudrun Magnusdottir**[1]

[1]Department of Earth System Science, University of California, Irvine, CA, USA

Abstract Recent modeling studies have shown an important role for stratosphere-troposphere coupling in the large-scale atmospheric response to Arctic sea ice loss. Evidence is growing that the Quasi-biennial Oscillation (QBO) can contribute to or even mitigate teleconnections from surface forcing. Here, the influence of QBO phase on the atmospheric response to projected Arctic sea ice loss is examined using an atmospheric general circulation model with a well-resolved stratosphere and a QBO prescribed from observations. The role of the QBO is determined by compositing seasons with easterly phase (QBO-E) separately from seasons with westerly phase (QBO-W). In response to the sea ice forcing in early winter, the polar vortex during QBO-E weakens with strong stratosphere-troposphere wave-1 coupling and a negative Northern Annular Mode-type response. At the surface, this results in more severe Siberian cold spells. For QBO-W, the polar vortex strengthens in response to the sea ice forcing.

Plain Language Summary Rapid loss of Arctic sea ice area and thickness are key indicators of global climate change. Global climate models project further loss of Arctic sea ice through the end of the 21st century. How weather patterns and the jet stream will respond to this sudden loss of sea ice is still poorly understood. Here we use a series of climate model experiments to understand how the atmospheric response to sea ice loss is affected by alternating easterly and westerly winds in the tropical middle atmosphere, known as the Quasi-biennial Oscillation. We show that the Quasi-biennial Oscillation has an important role in understanding how weather patterns can respond to a decrease in sea ice.

Key Points:
- Stratospheric response to different levels of sea ice decline is modulated by the Quasi-biennial Oscillation (QBO)
- A significant weakening of the polar vortex is only found under easterly QBO; the response is confined in the troposphere under westerly QBO
- Cold extremes over Eurasia intensify under easterly QBO due to a reinforcement of the Siberian High under stratosphere-troposphere coupling

Supporting Information:
- Supporting Information S1

Correspondence to:
Z. Labe,
zlabe@uci.edu

Citation:
Labe, Z., Peings, Y., & Magnusdottir, G. (2019). The effect of QBO phase on the atmospheric response to projected Arctic sea ice loss in early winter. *Geophysical Research Letters*, *46*, 7663–7671. https://doi.org/10.1029/2019GL083095

Received 30 MAR 2019
Accepted 17 JUN 2019
Accepted article online 24 JUN 2019
Published online 8 JUL 2019

1. Introduction

The pronounced warming in the Arctic over recent decades may affect not only the local climate but also midlatitude areas through atmospheric teleconnections (e.g., Cohen et al., 2014). The remote impact of Arctic sea ice loss is unclear due to divergence in the atmospheric response among modeling studies and low signal-to-noise ratio (e.g., Overland et al., 2016; Smith et al., 2019). However, recent coupled global climate model experiments, where sea ice is forced to substantially decrease by longwave radiative forcing (Tomas et al., 2016), albedo change (Blackport & Kushner, 2017), or by nudging (Smith et al., 2017), find robust response to the sea ice forcing as summarized in Screen et al. (2018).

Studies have pointed to the importance that the stratospheric circulation may play in shaping the response to sea ice forcing (e.g., Kim et al., 2014; Peings & Magnusdottir, 2014; Sun et al., 2015; Zhang et al., 2018). Anomalies in the polar stratosphere driven by wave breaking of surface-forced planetary waves affect the tropospheric circulation through the Northern Annular Mode (NAM; Baldwin & Dunkerton, 2001). Specifically, boundary conditions such as sea surface temperature (SST), sea ice concentration/sea ice thickness (SIC/SIT), or snow anomalies impact the polar stratosphere when the tropospheric anomalies they generate constructively interfere with the climatological stationary waves (Fletcher & Kushner, 2011; Henderson et al., 2018; Smith et al., 2011).

Any teleconnection that involves stratosphere-troposphere coupling may be impacted by the Quasi-biennial Oscillation (QBO), a ~28-month oscillation of the equatorial zonal wind in the stratosphere (Baldwin et al., 2001). As first hypothesized by Holton and Tan (1980), the QBO may affect the strength of the Northern Hemisphere polar vortex by altering the background flow and the propagation of extratropical planetary waves in the polar stratosphere. This mechanism is usually referred to as the Holton-Tan effect and is apparent in observations as well as model simulations (e.g., Anstey & Shepherd, 2014; Watson & Gray, 2014). Although the QBO is an important source of predictability for Northern Hemisphere winter surface

climate (Thompson et al., 2002), models generally simulate a weaker extratropical signal than in reanalysis (Andrews et al., 2019; Scaife et al., 2014). Further, the role of the QBO in modulating teleconnections related to surface forcings has received little attention. Some studies have explored how the QBO modulates the atmospheric response to Eurasian snow anomalies (Peings et al., 2017; Tyrrell et al., 2018), but to our knowledge no studies have evaluated its influence on the atmospheric response to Arctic sea ice change.

Here we address the role of the QBO in teleconnections involving surface forcing due to sea ice melt. We build primarily on two of the experiments considered in Labe et al. (2018) using a high-top atmospheric global climate model (AGCM) for forcing of SIC and SIT. In this work, we have extended the number of ensemble members for each experiment in Labe et al. (2018) from 100 to 200 and focus on the response in relation to QBO phase.

2. Methods, Model, and Experiments

The AGCM used in this study is the specified chemistry version of WACCM (SC-WACCM4; Smith et al., 2014). It includes CAM4 physics, 66 vertical levels (up to 5.1 $\times 10^{-6}$ hPa, ~140 km), and a parameterization of nonorographic gravity waves that contributes to the realistic frequency of stratospheric sudden warming events (Richter et al., 2010). The QBO is prescribed in the model by relaxing equatorial (between 22°S and 22°N) zonal winds from 86 to 4 hPa to the observed ~28-month cycle from radiosonde observations (Hansen et al., 2013). The horizontal resolution is 1.9° latitude by 2.5° longitude. Two ensembles of simulations are branched from a 200-year control as described in Peings et al. (2017).

Our model setup is the same as in Labe et al. (2018) but extended to 200 ensemble members per experiment to increase the number of seasons composited per QBO phase. Each simulation is prescribed with annually repeating cycles of SST, SIT, and SIC, which are taken from the mean of forty ensemble members from the fully coupled Community Earth System Model Large Ensemble (LENS; Kay et al., 2015). LENS uses historical forcing and then continues to the end of the 21st century under Representative Concentration Pathway 8.5. Earlier studies (e.g., Jahn et al., 2016; Labe et al., 2018) have demonstrated that LENS captures spatial patterns of sea ice variability quite well when compared with current satellite observations. Our two experiments represent sea ice conditions in the 1976–2005 observational period (hereafter, historical) and projected sea ice conditions during 2051–2080 (hereafter, future). Following convention, SSTs are set to historical values in all grid cells, except where SIC has changed by more than 10% in the future experiment. In these SIC loss areas, SST are set to the 2051–2080 LENS mean. A thorough description of these experiments can also be found in Labe et al., 2018's Table S1 (HIT for historical, FICT for future). Figures S1a–S1f in the supporting information show the difference in SIC and SIT between the future and historical experiments for October, November, and December. Widespread loss of SIC (~75–100%) is found in October and November with almost ice-free conditions across the Arctic Ocean (Figures S1a and S1b). The reduction in sea ice cover leads to an upward (positive) surface heat flux response in areas of thinner ice and newly open water, up to 100 W/m^2, primarily due to turbulent heat flux (Figures S1g–S1i).

The QBO index is defined as the average October to November 30-hPa zonal wind from 5°S to 5°N. We composite winters into easterly (QBO-E) or westerly (QBO-W) phases by the lower and upper terciles of the QBO index (i.e., approximately 67 winters per phase). As shown in Hansen et al. (2013) and Peings et al. (2017), SC-WACCM represents the Holton-Tan effect, with weaker (stronger) westerlies circling the polar vortex under QBO-E (QBO-W).

The atmospheric response to Arctic sea ice loss is obtained by subtracting the historical ensemble mean from the future ensemble mean after compositing by QBO phase. Statistical significance of the atmospheric response is determined using the two-sided Student's t test at the 95% confidence level, unless otherwise stated. Here we focus on the atmospheric response in early boreal winter (November to December) when the QBO influence is greatest in our model. This period is consistent with earlier studies showing a larger Holton-Tan effect in both observations and models in early winter (Anstey & Shepherd, 2014).

3. Large-Scale Atmospheric Response

3.1. Free Troposphere/Stratosphere Response

Figure 1 shows the December atmospheric response to the sea ice forcing (future minus historical) composited by QBO phase. The right-hand column shows the difference in response depending on QBO phase

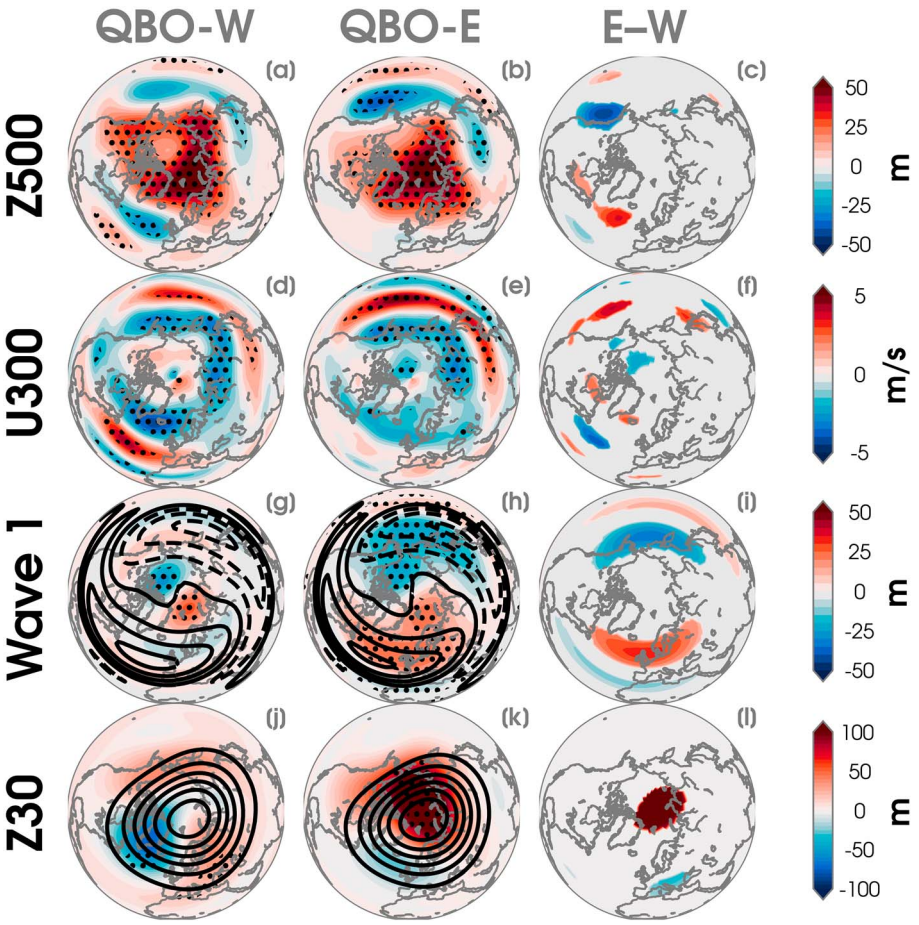

Figure 1. (a) December response to sea ice loss of the 500-hPa geopotential height (Z500) under QBO-W (Future-QBO-W minus Historical-QBO-W). (b) Same as (a), but for QBO-E. (c) Difference in the response under QBO-E minus QBO-W. Color shading indicates areas with at least 90% statistical significance. (d–f) Same as (a)–(c) but for the 300-hPa zonal wind (U300); (g–i) same as (a)–(c) but for the zonal Wave number 1 component of the 300-hPa geopotential height (Wave 1). The 300-hPa climatological Wave number 1 from the historical simulation is superimposed (50-m interval, black contours). (j–l) Same as (a)–(c) but for the 30-hPa geopotential height (Z30). The climatological Z30 heights from the historical simulation are superimposed (250-m interval, black contours). Black stippling is shown for statistically significant anomalies at the 95% confidence level in the first two columns. QBO = Quasi-biennial Oscillation; QBO-E = QBO easterly phase; QBO-W = QBO westerly phase.

(QBO-E minus QBO-W) and only areas that are statistically significant at the 90% confidence level are shaded. The overall tropospheric response corresponds to a negative NAM signature, with higher 500-hPa geopotential height (Z500) over the pole, and lower Z500 in midlatitudes (Figures 1a and 1b). This NAM response is stronger over the Atlantic for QBO-W (Figure 1a) and over the Pacific for QBO-E (Figure 1b) and is associated with equatorward shifts of the midlatitude jet streams (Figures 1d and 1e). While at first glance the two responses are similar, they project differently on the climatological stationary wave pattern. Under QBO-E, the tropospheric response reinforces Wave number 1 (Figure 1h), while this is not the case in QBO-W (Figure 1g). Therefore, QBO-E promotes constructive interference (Smith et al., 2011) and anomalous Rossby wave propagation into the stratosphere in December. Consistently, a warming of the polar stratosphere is found under QBO-E (Figures 1k and 1l), while QBO-W rather exhibits a cooling and a shift of the polar vortex toward the North Atlantic sector (Figure 1j). The statistical significance of the results in Figures 1j and 1k is also robust when using a 10,000 bootstrap resampling method instead of the two-sided Student's *t* test (black stippling).

The stratospheric response under QBO-E is consistent with constructive intereference between the forced Wave number 1 and the climatological stationary Wave 1 (Figure 1h). A more complete visual of linear interference between the forced and climatological stationary wave is provided in Figure S2. For QBO-E, there is

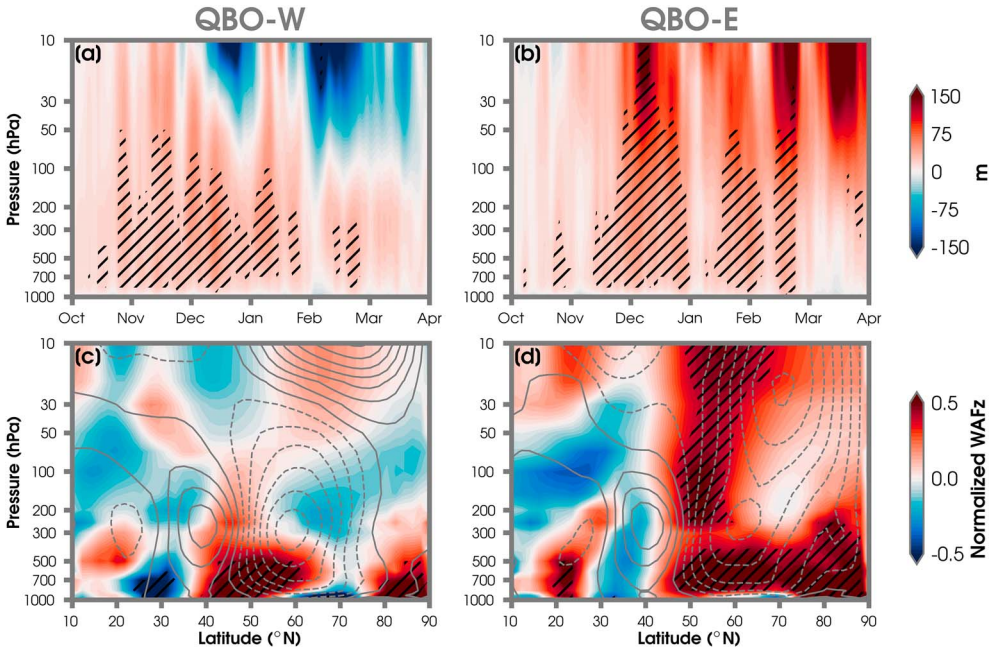

Figure 2. (a, b) Geopotential height response to sea ice decline as a function of height (pressure) over the polar cap (>65°N) for QBO-W (a) and QBO-E (b). Anomalies are shown from 1 October to 31 March. (c, d) Zonally averaged response (latitude-pressure vertical profile) of the normalized vertical wave activity flux averaged for November and December. The gray contours show the zonal-mean, zonal wind anomalies (0.25-m/s contour interval; dashed contours indicate negative values). Black hatch marks indicate statistical significance at the 95% confidence level. QBO = Quasi-biennial Oscillation; QBO-E = QBO easterly phase; QBO-W = QBO westerly phase.

large coherence between the climatological and forced Wave number 1 ($R = 0.87$), while for Wave number 2 the two fields are uncorrelated. This is consistent with other studies finding that the Holton-Tan effect is primarily driven by modulations of Wave number 1 in early winter (Hu & Tung, 2002; Ruzmaikin et al., 2005). For QBO-W (top), the correlation is considerably less for the total (left) and Wave number 1 (center) forced and climatological fields indicating there is less Wave number 1 propagation into the stratosphere. For Wave number 2 the spatial correlation is higher, but that is entirely due to values within the troposphere (right).

The daily evolution of the geopotential response to sea ice forcing, integrated over the polar cap (north of 65°N), is shown as a function of height in Figures 2a and 2b for October–March. For QBO-W, the statistically significant response is confined to the troposphere, with the positive polar geopotential response corresponding to the negative NAM observed in the midtroposphere in Figure 2a. In the stratosphere, the polar vortex strengthens through early winter, with little statistical significance in the anomalies. However, under QBO-E, there is a robust stratospheric response to the forcing in late November and December. This diagnostic clearly indicates that for QBO-E the stratospheric pathway has a role in the large-scale circulation response to the sea ice. While our focus is on early winter due to greater statistical significance, there is also a difference in the stratospheric response between QBO phases through the end of winter.

Figures 2c and 2d show the response of the November–December vertical component of the Eliassen-Palm flux (Plumb, 1985), equivalent to the meridional eddy heat flux, in a latitude-pressure cross section. The zonal-mean, zonal wind response in both QBO phases is also superimposed on the normalized flux anomalies. Both phases exhibit responses in the troposphere, with an equatorward shift of the westerlies, in line with previous studies that investigated the response to future Arctic sea ice loss (Labe et al., 2018; Screen et al., 2018). However, under QBO-E, the weakening of the westerlies extends to the stratosphere and is associated with increased vertical wave activity flux (WAFz) throughout the vertical column centered at 50°N (Figure 2d). In contrast, under QBO-W, the zonal-mean WAFz anomalies are confined in the troposphere (Figure 2c). The question is as follows: Under QBO-E conditions, where does this flux originate from? To answer that question, in Figure S3 we examine WAFz for the November–December response to sea ice forcing under QBO-W (left) and QBO-E (right). At 850 hPa under QBO-E, WAFz is positive largely in areas

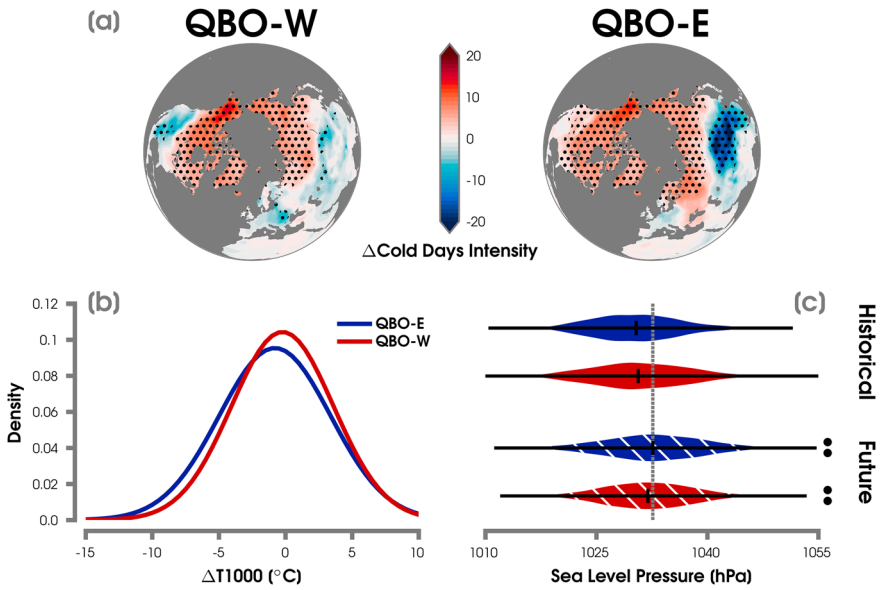

Figure 3. (a) Change in December cold day intensity for each QBO phase in response to sea ice decline. Statistical significance at the 95% confidence level is indicated by the black stippling. (b) The normalized probability density functions of the daily December temperature at 1,000-hPa (T1000) response to sea ice loss for Eurasia (35–60°N and 70–140°E). The T1000 responses are composed by the easterly (QBO-E; blue) and westerly (QBO-W; red) phases of the QBO. (c) Violin plots of the distributions of average daily sea level pressure over the Siberian High region (40–65°N and 80–120°E) in the historical and future experiments. Black lines show the median in each distribution. The dashed gray vertical line is displayed to highlight the median of the future QBO-E simulation. White hatch marks and the two black dots indicate a statistically significant difference in the means and between QBO-E and QBO-W composites in each experiment, respectively. QBO = Quasi-biennial Oscillation.

corresponding to the sea ice forcing. By contrast at 150 hPa, which is in the lower stratosphere, the area where the flux is strongly positive and statistically significant is in the area of the Siberian High. This flux is weaker and insignificant under QBO-W. We will look closer at this region and its importance for the response in the next section.

3.2. Surface Temperature Response

The concurrence of Arctic sea ice anomalies with recent cold extremes has led to the hypothesis that they may be causally related, that is, that Arctic sea ice loss may lead to winter cold extremes. However, linking sea ice loss to cold extremes and to the "warm Arctic, cold continent" spatial temperature pattern is not robust, neither in reanalysis nor in climate models (Barnes & Screen, 2015; Mori et al., 2014, 2019; Overland et al., 2011; Screen et al., 2015; Sun et al., 2016). Here we examine whether there is also a different signal at the surface depending on QBO phase.

Following the methods of Peings et al. (2018), we assess the change in cold temperature extremes by defining a cold days index (CDI; degree day). At each grid point, a December CDI is computed by summing each daily deviation of the 1,000-hPa temperature from its corresponding daily 10th percentile, based on the historical distribution. Therefore, this index captures both changes in frequency and intensity of cold extremes. Figure 3a shows a spatial map of the change in CDI due to sea ice loss and filtered by QBO phase. For both QBO-W and QBO-E there is a substantial reduction in CDI intensity (positive anomalies) over high-latitude North America and much of northern Eurasia during December. This is in response to warm air advection induced by sea ice loss. However, under QBO-E, there is a significant increase in CDI intensity (negative anomalies) over central and eastern Asia.

Figure 3b shows the probability density function for the daily December 1000-hPa temperature anomalies within the area of the cold patch in Figure 3a (35–60°N, 70–140°E). The Kolmogorov-Smirnov two-sample test is used to compare the shape of the distributions of the responses to sea ice loss under QBO-E and QBO-W. They are statistically different ($p < 0.001$), and for QBO-E the probability density function is shifted to cooler temperatures with an increased variance. Although this area of cooling is similar to the 2-m tem-

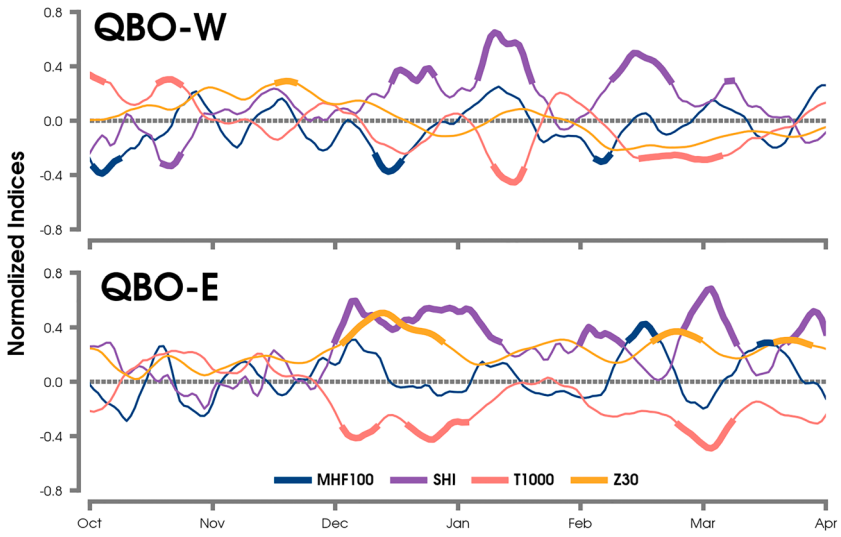

Figure 4. Daily time series of the zonal-average of the meridional eddy heat flux at 100 hPa (MHF100; blue line; 40–80°N), the Siberian High sea level pressure index (purple line; 40–65°N and 80–120°E), 1,000-hPa temperatures in Eurasia (T1000; red line; 35–60°N and 70–140°E), and the geopotential at 30 hPa averaged over the polar cap (Z30; orange line; >65°N) for QBO-W (top) and QBO-E (bottom) phases in response to sea ice loss. The fields have each been smoothed using a 10-day running average and normalized by their standard deviation. Statistical significance at the 90% confidence level is indicated by the bold line segments. QBO = Quasi-biennial Oscillation; QBO-E = QBO easterly phase; QBO-W = QBO westerly phase.

perature response in Labe et al. (2018), it is further amplified under QBO-E. These results suggest that the surface response to sea ice loss is modulated by the QBO and leads to an intensification of the cold temperature extremes under QBO-E.

The advection-induced cooling over central and eastern Asia is thought to arise from the intensification of the Siberian High (Mori et al., 2014). We show violin plots (Figure 3c) of the daily Siberian High Index (SHI) using sea level pressure averaged over 40–65°N and 80–120°E, which corresponds to the area of the Siberian High (Panagiotopoulos et al., 2005). The violin plots show the median SHI (center black lines) in addition to its kernel probability density symmetric around the 5th–95th percentile range (horizontal lines). We find a slightly stronger Siberian High response under QBO-E compared to QBO-W ($p < 0.001$). Note that under both QBO phases the Siberian High strengthens due to sea ice loss. This helps explain the similar location of the CDI minima for both QBO phases, although for QBO-E the amplitude is substantially larger.

An outstanding question is whether the stronger Siberian High response under QBO-E is driven by the polar vortex weakening. To investigate this question, Figure 4 shows daily time series of the responses in meridional eddy heat flux at 100 hPa ($\overline{v'T'}$; MHF100), SHI, 1,000-hPa temperature over Eurasia (T1000), and 30-hPa geopotential (Z30) averaged over the polar cap. During QBO-E in early December, positive MHF100 anomalies coincide with a strengthening of the SHI and decrease in mean temperature. This is followed by a stratospheric warming in mid-December, and persistent Siberian High and cold temperature anomalies in December (bottom). Over the entire season, the SHI is highly anticorrelated to T1000 ($R = -0.86$). Based on these results, we propose the following interpretation to explain how the QBO modulates the response to sea ice in our experiments: (1) the QBO modulates the Wave number 1 pattern response to sea ice anomalies (Figures 1g and 1h), (2) the enhancement of the Siberian High induces upward wave activity anomalies that lead to a warming of the polar stratosphere, and (3) the stratospheric anomaly propagates downward (Figure 2b) and reinforces the Siberian High/cold eastern Asia anomalies (Figure 3a). Thus, the Eurasian cooling is primarily driven by tropospheric processes, but the stratosphere reinforces the tropospheric response, leading to greater persistence in the Siberian High anomaly. Under QBO-W, episodes of strong SHI and T1000 are found, but they are less persistent, consistent with the absence of any stratospheric warming.

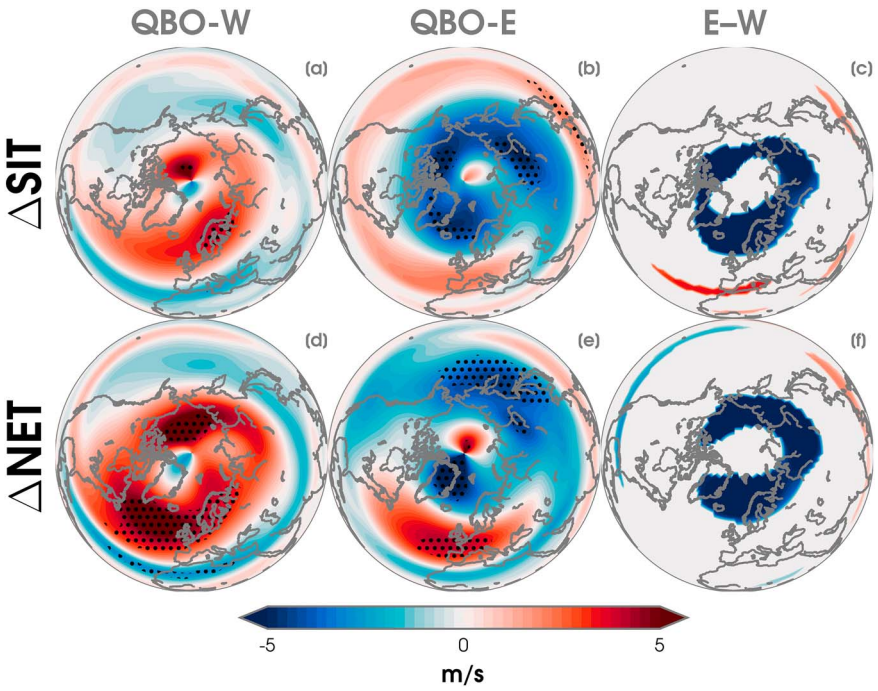

Figure 5. As in Figure 1, but for the December responses of the 10-hPa zonal wind in a sea ice thickness loss only experiment (*Δ*SIT; a–c) and the total sea ice change (concentration and thickness) experiment (*Δ*NET; d–f). QBO = Quasi-biennial Oscillation; QBO-E = QBO easterly phase; QBO-W = QBO westerly phase.

4. Conclusions

This illustrates for the first time how the QBO can modulate the atmospheric response to projected sea ice loss using perturbation experiments with a high-top AGCM (SC-WACCM4). A robust weakening of the polar vortex is found under QBO-E in response to sea ice decline. In contrast, there is a strengthening of the polar vortex under QBO-W. The total ensemble mean response shows a marginal strengthening of the stratospheric polar vortex as in Labe et al. (2018), due to the fact that neutral QBO years exhibit a strengthening of the polar vortex (not shown). However, a modulation of the response in the midtroposphere is not clear from this analysis.

The stratospheric response under QBO-E is driven by waves propagating into the stratosphere that coincide with the reinforcement of a Wave number 1 pattern and a stronger Siberian High response than under QBO-W. As a consequence, the warm Arctic-cold Siberia pattern is only statistically significant under QBO-E. These results illustrate how sensitive the large-scale response to Arctic sea ice is, even when using a strong forcing as in this study. Depending on the phase of the QBO, the conclusions significantly differ, which may be problematic in modeling studies that do not include a realistic QBO or are run under permanent QBO conditions. We also find that additional experiments forced by sea ice thickness only simulate a similar stratospheric response, despite much reduced heat flux anomalies at the surface (Labe et al., 2018, Figure 1d). Figure 5 shows the 10-hPa zonal wind response to a future SIT-only loss experiment (*Δ*SIT) compared with the SIC-SIT-loss experiment used in this study (*Δ*NET). Despite the much smaller forcing in *Δ*SIT, there is also a robust weakening of the polar vortex under QBO-E (Figure 5b). Further, the evolution of the daily time series fields for *Δ*SIT (not shown) are remarkably similar to those in Figure 4. Therefore, the response to Arctic sea ice loss is highly nonlinear, and the modulating role by the QBO may also intervene with smaller sea ice loss, although with weaker forcing internal variability cannot be ruled out. Note that the mechanisms leading to the influence of the QBO on the climatological stationary wave pattern are still under investigation.

Such strong dependence to seemingly minor changes in the experiment protocol suggests the importance of the model mean state regarding its sensitivity to sea ice anomalies. Along with other parameters that influence the model mean state, for example, background SST (Osborne et al., 2017; Smith et al., 2017), inconsistent representation of the QBO may lead to discrepancies among modeling studies (Overland et al.,

2016; Screen et al., 2018). In that context, it is well established that accompanying a change in phase of the QBO are changes in the mean circulation such as strength of the stratospheric polar vortex and even the character of the tropospheric jets (Kidston et al., 2015). The sensitivity that we find in the sea ice loss experiments is associated with QBO phase since the sea ice forcing is strong enough, and the number of ensemble members is great enough that we can rule out internal variability. Most models still struggle to produce a realistic internally generated QBO (Schenzinger et al., 2017), and our results suggest this may affect how they respond to Arctic sea ice or other boundary conditions. At this stage, we do not know whether other GCMs exhibit similar sensitivity to the QBO.

Acknowledgments
Computing support is provided through NCAR, sponsored by the National Science Foundation (NSF; https://doi.org/10.5065/D6RX99HX). We thank two anonymous reviewers for their insightful comments to improve this study. CESM-LENS sea ice data are available at http://www.cesm.ucar.edu/projects/community-projects/LENS/data-sets.html website. Outputs from the AGCM simulations are available from the corresponding author and stored on Cheyenne's High Performance Storage System long-term data archive. This study was supported by DOE Grant DE-SC0019407, NOAA Grant NA15OAR4310164, and NSF Grants AGS-1624038 and NRT-1633631.

References

Andrews, M. B., Knight, J. R., Scaife, A. A., Lu, Y., Wu, T., Gray, L. J., & Schenzinger, V. (2019). Observed and simulated teleconnections between the stratospheric Quasi-Biennial Oscillation and Northern Hemisphere winter atmospheric circulation. *Journal of Geophysical Research: Atmospheres*, *124*, 1219–1232. https://doi.org/10.1029/2018JD029368

Anstey, J. A., & Shepherd, T. G. (2014). High-latitude influence of the quasi-biennial oscillation. *Quarterly Journal of the Royal Meteorological Society*, *140*(678), 1–21. https://doi.org/10.1002/qj.2132

Baldwin, M. P., & Dunkerton, T. J. (2001). Stratospheric harbingers of anomalous weather regimes. *Science (New York, N.Y.)*, *294*(5542), 581–584. https://doi.org/10.1126/science.1063315

Baldwin, M. P., Gray, L. J., Dunkerton, T. J., Hamilton, K., Haynes, P. H., Randel, W. J., et al. (2001). The quasi-biennial oscillation. *Reviews of Geophysics*, *39*(2), 179–229. https://doi.org/10.1029/1999RG000073

Barnes, E. A., & Screen, J. A. (2015). The impact of Arctic warming on the midlatitude jet-stream: Can it? Has it? Will it? *Wiley Interdisciplinary Reviews: Climate Change*, *6*(3), 277–286. https://doi.org/10.1002/wcc.337

Blackport, R., & Kushner, P. J. (2017). Isolating the atmospheric circulation response to Arctic sea ice loss in the coupled climate system. *Journal of Climate*, *30*(6), 2163–2185. https://doi.org/10.1175/JCLI-D-16-0257.1

Cohen, J., Screen, J. A., Furtado, J. C., Barlow, M., Whittleston, D., Coumou, D., et al. (2014). Recent Arctic amplification and extreme mid-latitude weather. *Nature Geoscience*, *7*(9), 627–637. https://doi.org/10.1038/ngeo2234

Fletcher, C. G., & Kushner, P. J. (2011). The role of linear interference in the annular mode response to tropical SST forcing. *Journal of Climate*, *24*(3), 778–794. https://doi.org/10.1175/2010JCLI3735.1

Hansen, F., Matthes, K., & Gray, L. J. (2013). Sensitivity of stratospheric dynamics and chemistry to QBO nudging width in the chemistry-climate model WACCM. *Journal of Geophysical Research: Atmospheres*, *118*, 10,464–10,474. https://doi.org/10.1002/jgrd.50812

Henderson, G. R., Peings, Y., Furtado, J. C., & Kushner, P. J. (2018). Snow-atmosphere coupling in the Northern Hemisphere. *Nature Climate Change*, *18*(11), 954–963. https://doi.org/10.1038/s41558-018-0295-6

Holton, J. R., & Tan, H. C. (1980). The influence of the equatorial Quasi-Biennial Oscillation on the global circulation at 50 mb. Retrieved from https://doi.org/10.1175/1520-0469(1980)037<2200:TIOTEQ>2.0.CO;2

Hu, Y., & Tung, K. K. (2002). Tropospheric and equatorial influences on planetary-wave amplitude in the stratosphere. *Geophysical Research Letters*, *29*(2), 1019. https://doi.org/10.1029/2001GL013762

Jahn, A., Kay, J. E., Holland, M. M., & Hall, D. M. (2016). How predictable is the timing of a summer ice-free Arctic? *Geophysical Research Letters*, *43*, 9113–9120. https://doi.org/10.1002/2016GL070067

Kay, J. E., Deser, C., Phillips, A., Mai, A., Hannay, C., Strand, G., et al. (2015). The Community Earth System Model (CESM) large ensemble project: A Community Resource for Studying Climate Change in the presence of internal climate variability. *Bulletin of the American Meteorological Society*, *8*, 1333–1349. https://doi.org/10.1175/BAMS-D-13-00255.1

Kidston, J., Scaife, A. A., Hardiman, S. C., Mitchell, D. M., Butchart, N., Baldwin, M. P., & Gray, L. J. (2015). Stratospheric influence on tropospheric jet streams, storm tracks and surface weather. *Nature Geoscience*, *8*(6), 433–440. https://doi.org/10.1038/ngeo2424

Kim, B.-M., Son, S.-W., Min, S.-K., Jeong, J.-H., Kim, S.-J., Zhang, X., et al. (2014). Weakening of the stratospheric polar vortex by Arctic sea-ice loss. *Nature Communications*, *5*, 4646. https://doi.org/10.1038/ncomms5646

Labe, Z., Magnusdottir, G., & Stern, H. (2018). Variability of Arctic sea ice thickness using PIOMAS and the CESM large ensemble. *Journal of Climate*, *31*(8), 3233–3247. https://doi.org/10.1175/JCLI-D-17-0436.1

Labe, Z., Peings, Y., & Magnusdottir, G. (2018). Contributions of ice thickness to the atmospheric response from projected Arctic sea ice loss. *Geophysical Research Letters*, *45*, 5635–5642. https://doi.org/10.1029/2018GL078158

Mori, M., Kosaka, Y., Watanabe, M., Nakamura, H., & Kimoto, M. (2019). A reconciled estimate of the influence of Arctic sea-ice loss on recent Eurasian cooling. *Nature Climate Change*, *9*, 123–129. https://doi.org/10.1038/s41558-018-0379-3

Mori, M., Watanabe, M., Shiogama, H., Inoue, J., & Kimoto, M. (2014). Robust Arctic sea-ice influence on the frequent Eurasian cold winters in past decades. *Nature Geoscience*, *7*(12), 869–873. https://doi.org/10.1038/ngeo2277

Osborne, J. M., Screen, J. A., & Collins, M. (2017). Ocean-atmosphere state dependence of the atmospheric response to Arctic sea ice loss. *Journal of Climate*, *30*(5), 1537–1552. https://doi.org/10.1175/JCLI-D-16-0531.1

Overland, J. E., Dethloff, K., Francis, J. A., Hall, R. J., Hanna, E., Kim, S.-J., et al. (2016). Nonlinear response of mid-latitude weather to the changing Arctic. *Nature Climate Change*, *6*(11), 992–999. https://doi.org/10.1038/nclimate3121

Overland, J. E., Wood, K. R., & Wang, M. (2011). Warm Arctic-cold continents: Climate impacts of the newly open Arctic Sea. *Polar Research*, *30*(1), 15787. https://doi.org/10.3402/polar.v30i0.15787

Panagiotopoulos, F., Shahgedanova, M., Hannachi, A., & Stephenson, D. B. (2005). Observed trends and teleconnections of the Siberian High: A recently declining center of action. *Journal of Climate*, *18*(9), 1411–1422. https://doi.org/10.1175/JCLI3352.1

Peings, Y., Cattiaux, J., Vavrus, S. J., & Magnusdottir, G. (2018). Projected squeezing of the wintertime North-Atlantic jet. *Environmental Research Letters*, *13*(7), 74016. https://doi.org/10.1088/1748-9326/aacc79

Peings, Y., Douville, H., Colin, J., Martin, D. S., & Magnusdottir, G. (2017). Snow-(N)AO teleconnection and its modulation by the Quasi-Biennial Oscillation. *Journal of Climate*, *30*(24), 10,211–10,235. https://doi.org/10.1175/JCLI-D-17-0041.1

Peings, Y., & Magnusdottir, G. (2014). Response of the wintertime Northern Hemisphere atmospheric circulation to current and projected Arctic sea ice decline: A numerical study with CAM5. *Journal of Climate*, *27*(1), 244–264. https://doi.org/10.1175/JCLI-D-13-00272.1

Plumb, R. A. (1985). On the three-dimensional propagation of stationary waves. *Journal of the Atmospheric Sciences*, *42*(3), 217–229. https://doi.org/10.1175/1520-0469(1985)042<0217:OTTDPO>2.0.CO;2

Richter, J. H., Sassi, F., & Garcia, R. R. (2010). Toward a physically based gravity wave source parameterization in a General Circulation Model. *Journal of the Atmospheric Sciences*, *67*(1), 136–156. https://doi.org/10.1175/2009JAS3112.1

Ruzmaikin, A., Feynman, J., Jiang, X., & Yung, Y. L. (2005). Extratropical signature of the quasi-biennial oscillation. *Journal of Geophysical Research*, *110*, D11111. https://doi.org/10.1029/2004JD005382

Scaife, A. A., Athanassiadou, M., Andrews, M., Arribas, A., Baldwin, M., Dunstone, N., et al. (2014). Predictability of the quasi-biennial oscillation and its northern winter teleconnection on seasonal to decadal timescales. *Geophysical Research Letters*, *41*, 1752–1758. https://doi.org/10.1002/2013GL059160

Schenzinger, V., Osprey, S., Gray, L., & Butchart, N. (2017). Defining metrics of the Quasi-Biennial Oscillation in global climate models. *Geoscientific Model Development*, *10*(6), 2157–2168. https://doi.org/10.5194/gmd-10-2157-2017

Screen, J. A., Deser, C., Smith, D. M., Zhang, X., Blackport, R., Kushner, P. J., et al. (2018). Consistency and discrepancy in the atmospheric response to Arctic sea-ice loss across climate models. *Nature Geoscience*, *11*(3), 155–163. https://doi.org/10.1038/s41561-018-0059-y

Screen, J. A., Deser, C., & Sun, L. (2015). Reduced risk of North American cold extremes due to continued Arctic sea ice loss. *Bulletin of the American Meteorological Society*, *96*(9), 1489–1503. https://doi.org/10.1175/BAMS-D-14-00185.1

Smith, D. M., Dunstone, N. J., Scaife, A. A., Fiedler, E. K., Copsey, D., & Hardiman, S. C. (2017). Atmospheric response to Arctic and Antarctic sea ice: The importance of ocean-atmosphere coupling and the background state. *Journal of Climate*, *30*(12), 4547–4565. https://doi.org/10.1175/JCLI-D-16-0564.1

Smith, K. L., Kushner, P. J., & Cohen, J. (2011). The role of linear interference in Northern Annular Mode variability associated with Eurasian snow cover extent. *Journal of Climate*, *24*(23), 6185–6202. https://doi.org/10.1175/JCLI-D-11-00055.1

Smith, K. L., Neely, R. R., Marsh, D. R., & Polvani, L. M. (2014). The Specified Chemistry Whole Atmosphere Community Climate Model (SC-WACCM). *Journal of Advances in Modeling Earth Systems*, *6*, 883–901. https://doi.org/10.1002/2014MS000346

Smith, D. M., Screen, J. A., Deser, C., Cohen, J., Fyfe, J. C., García-Serrano, J., et al. (2019). The Polar Amplification Model Intercomparison Project (PAMIP) contribution to CMIP6: Investigating the causes and consequences of polar amplification. *Geoscientific Model Development*, *12*(3), 1139–1164. https://doi.org/10.5194/gmd-12-1139-2019

Sun, L., Deser, C., & Tomas, R. A. (2015). Mechanisms of stratospheric and tropospheric circulation response to projected Arctic sea ice loss* *Journal of Climate*, *28*(19), 7824–7845. https://doi.org/10.1175/JCLI-D-15-0169.1

Sun, L., Perlwitz, J., & Hoerling, M. (2016). What caused the recent "Warm Arctic, Cold Continents" trend pattern in winter temperatures? *Geophysical Research Letters*, *43*, 5345–5352. https://doi.org/10.1002/2016GL069024

Thompson, D. W. J., Baldwin, M. P., & Wallace, J. M. (2002). Stratospheric connection to Northern Hemisphere wintertime weather: Implications for prediction. *Journal of Climate*, *15*(12), 1421–1428. https://doi.org/10.1175/1520-0442(2002)015<1421:SCTNHW>2.0.CO;2

Tomas, R. A., Deser, C., & Sun, L. (2016). The role of ocean heat transport in the global climate response to projected Arctic sea ice loss. *Journal of Climate*, *19*, 6841–6859. https://doi.org/10.1175/JCLI-D-15-0651.1

Tyrrell, N. L., Karpechko, A. Y., & Räisänen, P. (2018). The influence of Eurasian snow extent on the northern extratropical stratosphere in a QBO resolving model. *Journal of Geophysical Research: Atmospheres*, *123*, 315–328. https://doi.org/10.1002/2017JD027378

Watson, P. A. G., & Gray, L. J. (2014). How does the Quasi-Biennial Oscillation affect the stratospheric polar vortex? *Journal of the Atmospheric Sciences*, *71*(1), 391–409. https://doi.org/10.1175/JAS-D-13-096.1

Zhang, P., Wu, Y., Simpson, I. R., Smith, K. L., Zhang, X., De, B., & Callaghan, P. (2018). A stratospheric pathway linking a colder Siberia to Barents-Kara Sea sea ice loss. *Science Advances*, *4*(7), eaat6025. https://doi.org/10.1126/sciadv.aat6025